Effect of Ion Exchange on the Adsorption of Steam Methane Reforming Off-Gases on Zeolite 13X

Filipe V. S. Lopes, Carlos A. Grande, Ana M. Ribeiro, Vítor J. P. Vilar, José M. Loureiro, and Alírio E. Rodrigues*

Laboratory of Separation and Reaction Engineering (LSRE), Associate Laboratory LSRE-LCM, Department of Chemical Engineering, Faculty of Engineering, University of Porto (FEUP), Rua Dr. Roberto Frias, s/n, 4200-465, Porto, Portugal

In this study, we have modified a material with enhanced adsorption capacity and kinetics toward nitrogen to apply in a layered pressure swing adsorption (PSA) unit for separation of steam methane reforming (SMR) off-gases. The adsorption properties of the base zeolite 13X (sodium form) were modified by changing the cation with lithium, barium, and calcium. The best adsorbent was selected by determining the difference in adsorption capacity measured by breakthrough experiments with (0.01 and 0.25) bar of partial pressure of nitrogen (effective capacity in a PSA unit) and the crystal diffusivity [at (303 and 323) K]. The ion exchange of zeolite 13X with Ba^{2+} and Ca^{2+} will favor nitrogen adsorption, with the calcium-modified sample having better performance (higher adsorption capacity). Adsorption equilibrium and kinetics of N_2, H_2, CO, CH_4, and CO_2 on ion-exchanged zeolite 13X-Ca were studied at (303 and 323) K in the pressure range (0 to 7) bar. At 1 bar of N_2, the loading of the 13X-Ca was 0.447 mol·kg^{-1} against 0.288 mol·kg^{-1} of the original 13X-Na zeolite.

1. Introduction

Hydrogen is the energy carrier of the future. It can be employed in stationary sources for energy production, and it is nowadays produced employing the steam reforming of hydrocarbons, normally methane.[1−4] The steam methane reforming (SMR) reactor produces a gas mixture containing high amounts of hydrogen [(70 to 72) %] and (15 to 20) % of carbon dioxide, and it is saturated with water and also contaminated with carbon monoxide (< 4 %) and unreacted methane (< 8 %). Also, if the methane employed as fuel is contaminated with nitrogen, this gas will also be part of the off-gases (< 4 %).[5] To purify the hydrogen from this complex mixture, a layered pressure swing adsorption (PSA) unit is commonly used.[1,2,4−12] A first adsorbent layer composed by activated carbon removes the heavier contaminants (H_2O, CO_2, and CH_4—high carbon dioxide and methane capacities and regenerability and water tolerance). A second material, usually zeolite, removes the lighter compounds (remaining methane, carbon monoxide, and nitrogen).[8,9] For correct PSA operation, CO_2 cannot be adsorbed in the zeolite layer since its desorption will be extremely difficult. Several experimental and theoretical studies of adsorption data for H_2 purification through PSA are reported in the literature.[1,5,8,10,12−16] However, these studies frequently do not consider a complete full set of gases (H_2, CO_2, and the impurities CH_4, CO, and N_2). When all gases are considered,[2,4,7,11] these studies are mainly for activated carbons and/or zeolite 5A. Conversely, adsorption studies with different zeolites and feeds including nitrogen are normally contemplated in air purification processes, which are not representative of hydrogen purification from the gases exiting a SMR reactor. Thus, as zeolites are widely used as the second adsorbent layer in a PSA process for hydrogen purification, fundamental studies dealing with adsorption properties of CO_2, H_2, CH_4, CO, and N_2 are lacking in the literature which is the focus of this work.

Zeolites are microporous crystalline solids with neutral SiO_2 groups and negatively charged $(AlO_2)^-$ compensated by a nonframework cation (Na^+, Li^+, Ba^{2+}, and/or Ca^{2+}).[17−19] These cations interact with the gas molecules that we want to separate and are responsible for the selectivity of the material.[18,19] These charge-balancing cations can be permuted through ion exchange.[20] To reach total or high exchange levels with simplicity and reproducibility, this method should be repeated several times (it essentially depends on the amount of cations present in solution), involving handling and recycling of large volumes of solution.[21] Another procedure to reach high levels of exchange is to pass a continuous flow of calcium solution through a column filled with zeolite until the exchange is completed.

In H_2 purification by PSA, nitrogen is the lighter contaminant and the first one to break through. This is the reason why improving the capacity of the adsorbents toward this gas will increase the productivity of the unit. When N_2 is not present, the extent of the feed step is determined by CH_4 and CO.[22] Many authors reported different types of ion exchange of a zeolite to allow the enhancement of the nitrogen selectivity.[22−25] Calcium and barium were employed for this purpose.[22] Significant enhancements were reported for zeolites with more than 50 % of exchanged calcium ions.[25] Different types of lithium exchanged zeolite X with different ion exchange ratios were also suggested in the literature due to their higher adsorption capacities for nitrogen and carbon monoxide. It was reported that a binary ion exchanged zeolite of type X with lithium and calcium (85 % of Li^+ and 15 % of Ca^{2+}; instead of calcium it could also be strontium) had the best performance to enhance the N_2 adsorption capacity.[23] Moreover, Plee (2002)[24] mentioned

* To whom correspondence should be addressed. Phone: +351 22 508 1671. Fax: +351 22 508 1674. E-mail: arodrig@fe.up.pt.

10.1021/je900303y CCC: $40.75
Published on Web 09/22/2009

Table 1. Experimental Conditions Used on the Measurement of the Breakthrough Curves of N_2 (1.0 % and 25.0 % of N_2 Balanced in He) in Zeolites 13X, 13X-Li, 13X-Ba, and 13X-Ca and of CO_2, CH_4, CO (0.5 % of Adsorbate Balanced in He) and Pure H_2 in Zeolite 13X-Ca at (303 and 323) K and 1 bar of Total Pressure

adsorbate	N_2				CO_2, CH_4, CO, and H_2
partial pressure [bar]	0.010, 0.250				0.005, 1[a]
adsorbent	13X	13X-Li	13X-Ba	13X-Ca	13X-Ca
mass of adsorbent $\times 10^3$ [kg]	9.118	6.948	8.597	7.863	4.498
bed height [m]	0.165	0.134	0.139	0.139	0.080
bed volume $\times 10^5$ [m^3]	1.245	1.012	1.048	1.048	0.6034
bed porosity, ε	0.396	0.397	0.395	0.395	0.399
pellet porosity, ε_p	0.394	0.431	0.322	0.380	0.380
adsorbent density, ρ_p[kg·m^{-3}]	1212	1138	1356	1241	1241

solid density, $\rho_s = 2000$ kg·m^{-3}; crystal diameter, $r_c = \sim 1.5$ μm; average pellet radius, $R_p = 8.5 \cdot 10^{-4}$ m; average pellet length, $L_p = \sim 5 \cdot 10^{-2}$ m

[a] The adsorbate partial pressure is 1 bar for H_2; for the other gases, it is 0.005 bar.

that a binary lithium and calcium ion exchanged zeolite for a Li/(Li + Ca) ratio higher than 0.7 is preferable for nitrogen adsorption.

The purpose of this work is to provide fundamental adsorption data of SMR off-gases (CO_2, H_2, CH_4, CO, and N_2) on ion exchange zeolite 13X with enhanced adsorption capacity and kinetics toward nitrogen. Three samples of exchanged zeolites were prepared starting from a commercial zeolite 13X and then characterized. Diffusion parameters of nitrogen in zeolite 13X and the three exchanged zeolites at (303 and 323) K were determined. A selection of the "best" adsorbent for N_2 adsorption was based on the difference between the amount of gas adsorbed at the highest and lowest adsorbate partial pressures, which in this case are (0.25 and 0.01) bar. The difference between these amounts will be termed as "useful capacity". The adsorbent chosen was the one with the "best" performance (higher adsorption capacity): 13X-Ca. Adsorption equilibrium and kinetics of N_2, CO_2, CH_4, CO, and H_2 on the 13X-Ca were studied at (0 to 7) bar and (303 and 323) K.

2. Experimental Section

2.1. Ion Exchange. Three different samples were prepared by exchanging 10.0 g (± 10^{-5} g) of zeolite 13X extrudates (Trade/Shanli, China) with lithium, calcium, and barium. To exchange the samples with Li^+, Ca^{2+}, or Ba^{2+} ions with a proportion of 20.0 $mL_{solution} \cdot g_{zeolite}^{-1}$, three 1 N solutions of 200 mL (± 0.10 mL) were prepared in deionized water: one with LiCl, a second with $Ca(NO_3)_2$, and another with $BaCl_2$. Each sample was introduced into an Erlenmeyer with 50 mL (± 0.05 mL) of the respective cationic solution. The three Erlenmeyer flasks were placed in a shaker for 12 h, at 313 K (± 0.1 K). The solid and liquid phases present in the flasks were separated by filtration. This procedure was repeated three more times to reach 200 mL of cationic solution used in each sample. At the end of the fourth batch, the two phases present in the Erlenmeyers were separated by filtration, and then the samples (solid phase) were dried in an oven at 373 K (± 0.1 K) for 1 day.

For the zeolite 13X and for three samples of exchanged zeolites 13X (13X-Li, 13X-Ba, and 13X-Ca), the morphology of the particles was observed by scanning electron microscopy (SEM). Semiquantitative elemental composition was determined by an energy dispersive X-ray (EDX).

A scale-up protocol to exchange 80 g/batch (± 10^{-5} g/batch) of exchanged zeolite 13X sample with the highest performance for nitrogen (adsorbent with higher N_2 adsorption capacity) was performed using similar experimental conditions as detailed previously. In the scale-up protocol, 400 mL (± 0.30 mL) of 1 N cationic solution was used in the four exchange batches. During the scale-up procedure, the concentration history of the Na^+ cations in the supernatants was determined by atomic absorption spectrometry (GBC 932 Plus Atomic Absorption Spectrometer). The working current/wavelength was adjusted to 5.0 mA/330.2 nm, giving a detection limit of 4 mg·L^{-1}. The instrument response was periodically checked with Na^+ solution standards. This procedure allowed the calculation of the final total concentration of exchanged cations on the structure of the modified zeolite material.

2.2. Nitrogen Adsorption on Ion Exchanged Zeolites. The adsorption equilibrium of pure nitrogen on the samples of zeolites 13X, 13X-Li, 13X-Ba, and 13X-Ca was studied by chromatographic technique measurements of two sets of breakthrough curves at (303 and 323) K (± 0.1 K) and atmospheric pressure: one set with mixtures of 1.0 % of nitrogen and another of 25.0 % of nitrogen, both balanced with helium. The bed outlet concentration was measured by TCD (thermal conductivity detector) installed in the gas chromatograph where the column was placed. The experimental conditions used in these measurements and the dimensions of the column are given in Table 1. The breakthrough experiments performed with the mixture of 1.0 % N_2 balanced in He were also used to determine the transport kinetics of nitrogen in the four samples through moment analysis of the pulse response, i.e., derivative of the diluted breakthrough curve. The crystal diffusivities were calculated based on the experimental values of the moments (derived from the solution in Laplace form by the application of van der Laan's theorem) together with estimated values of axial dispersion coefficients, molecular and macropore diffusivities (according to the correlations given in Table 2).[26−28] Employing this highly diluted mixture (N_2 partial pressure of 0.01 bar), we will not have the effect of isotherm nonlinearity, and we ensure isothermal conditions with an almost constant flow rate.

Similar breakthrough curves using 0.5 % of gas diluted in helium were performed to determine the transport kinetics of carbon dioxide, methane, and carbon monoxide in the sample with the highest adsorption capacity for nitrogen (Tables 1 and 2).[26−28] Pure breakthrough curves of H_2 were performed since H_2 isotherms are linear in the pressure range (0 to 1) bar.

To degass the sample of zeolite 13X and the ion-exchanged samples of zeolite 13X, a helium flow of $6.25 \cdot 10^{-7}$ $m^3 \cdot s^{-1}$ (measured at 298 K) was used overnight at 593 K (± 0.1 K), after heating at 1 K·min^{-1} (± 0.1 K·min^{-1}) from 298 K.

2.3. Adsorption Equilibrium of N_2, CO_2, CH_4, CO, and H_2. Adsorption equilibrium isotherms of N_2, CO_2, CH_4, CO, and H_2 were measured for the exchanged zeolite 13X sample with the highest performance for nitrogen. The adsorption equilibrium measurements were performed in a magnetic

suspension microbalance (Rubotherm, Germany) (± 10^{-5} g) at (303 and 323) K (± 0.1 K) within (0 to 7) bar (± 0.0014 bar). Degassing of the sample was carried out with a heating rate of 1 K·min^{-1} (± 0.1 K·min^{-1}) under vacuum (<10^{-7} bar) at 593 K (± 0.1 K) overnight. Adsorption and desorption measurements were performed to confirm the reversibility of each isotherm.

The absolute amount adsorbed was calculated by correcting the experimental data with buoyancy effects by[29]

$$q = \frac{\Delta m + \rho_g(V_s + V_c)}{m_s M_W}\frac{\rho_{/}}{\rho_{/} - \rho_g} \quad (1)$$

where it is assumed that the density of the adsorbed phase is equal to the density of the liquid at its boiling point at 1 atm.[30] The terms in this and the subsequent equations are defined in the Nomenclature.

The experimental adsorption equilibrium data were fitted with the virial adsorption isotherm model. This model is obtained by applying the bidimensional virial equation of state to the Gibbs isotherm[31,32]

$$P = \frac{q}{K_H}\exp\left(\frac{2}{S}Aq + \frac{3}{2S^2}Bq^2 + ...\right) \quad (2)$$

where S is the adsorbent-specific surface area; K_H is the Henry constant; and A and B are virial coefficients. The Henry constant is temperature dependent through the van't Hoff equation

$$K_H = K_\infty \exp\left(\frac{-\Delta H}{R_g T}\right) \quad (3)$$

The virial adsorption isotherm model can be truncated after the second virial coefficient. These coefficients are also related to temperature through the equations

$$A = \sum_{m=0}^{\infty}\frac{A_m}{T^m},\ B = \sum_{m=0}^{\infty}\frac{B_m}{T^m} \quad (4)$$

An extension of the virial isotherm was reported by Taqvi and LeVan (1997) for prediction of multicomponent adsorption.[33]

The fitting was performed using MATLAB (The MathWorks, Inc.), by minimization of an error function with a precision of 10^{-16} for all the variables involved. The error function defined was[34,35]

$$\mathrm{ERR} = \frac{(1-w)}{N}\sum_T\sum_q\left(\frac{P_{exp} - P_{cal}}{P_{exp}}\right)^2 + w\sum_T\sum_q(P_{exp} - P_{cal})^2 \quad (5)$$

where T is each experimental temperature; q is the adsorbed phase concentration; N is the number of points of each isotherm; P_{exp} is the experimental partial pressure; P_{cal} is the calculated partial pressure; and the parameter w is between 0 and 1.

The isosteric heats of adsorption were calculated through the Clausius−Clapeyron equation, where the derivative has to be evaluated at a constant amount adsorbed q

$$(-\Delta H_i) = R_g T^2\left(\frac{\partial \ln P_i}{\partial T}\right)_q \quad (6)$$

Plotting ln P versus $1/T$, a straight line equation with slope equal to $(-\Delta H_i)/R_g$ is obtained.

3. Results and Discussion

3.1. Ion Exchange. The scanning electron microscopy (SEM) images used to determine the morphology of the particles of

Table 2. Moment Analysis Based on the Pulse Response (Derivative of Diluted Breakthrough Curves) and Correlations Used to Estimate the Diffusivity Constants

first moment	$\mu_1 = \frac{L}{u_i}\left(1 + \left(\frac{1-\varepsilon}{\varepsilon}\right)K_H\rho_p R_g T\right)$
ratio of the variance and 2 times the first moment square	$\frac{\sigma^2}{2{\mu_1}^2} = \frac{D_{ax}}{u_i L} + \left(\frac{u_i}{L}\right)\left(\frac{\varepsilon}{1-\varepsilon}\right)\left(\frac{R_p}{2k_f} + \frac{R_p^2}{\Omega_p\varepsilon_p D_p} + \frac{r_c^2}{\Omega_c K_H D_c}\right)\cdot\left(1 + \frac{\varepsilon_p}{(1-\varepsilon_p)K_H\rho_p R_g T}\right)^{-2}$
	with $K_H \gg \varepsilon_p$; zeolite: $\Omega_p = 8$(cylinder particles); $\Omega_c = 15$ (spherical crystals)
axial dispersion	$D_{ax} = (0.45 + 0.55\varepsilon)D_m + 0.35R_p u_i$
film mass transfer	$Sh = 2.0 + 1.1Re^{0.6}Sc^{1/3}$
	with $Sh = 2R_p k_f/D_m$, $Re = 2\rho_g u_0 R_p/\mu$, and $Sc = \mu/\rho_g D_m$
Bosanquet equation	$\frac{1}{D_p} = \tau_p\left(\frac{1}{D_m} + \frac{1}{D_k}\right)$
Wilke correlation (molecular diffusion coefficients)	$D_m = \frac{1-y_i}{\sum_{\substack{j=1\\ j\neq i}}^{n}\frac{y_i}{D_{ij}}}$
Knudsen diffusivity (m^2·s^{-1})	$D_k = 97.0 r_p\sqrt{\frac{T}{M_W}}$ with r_p in meters

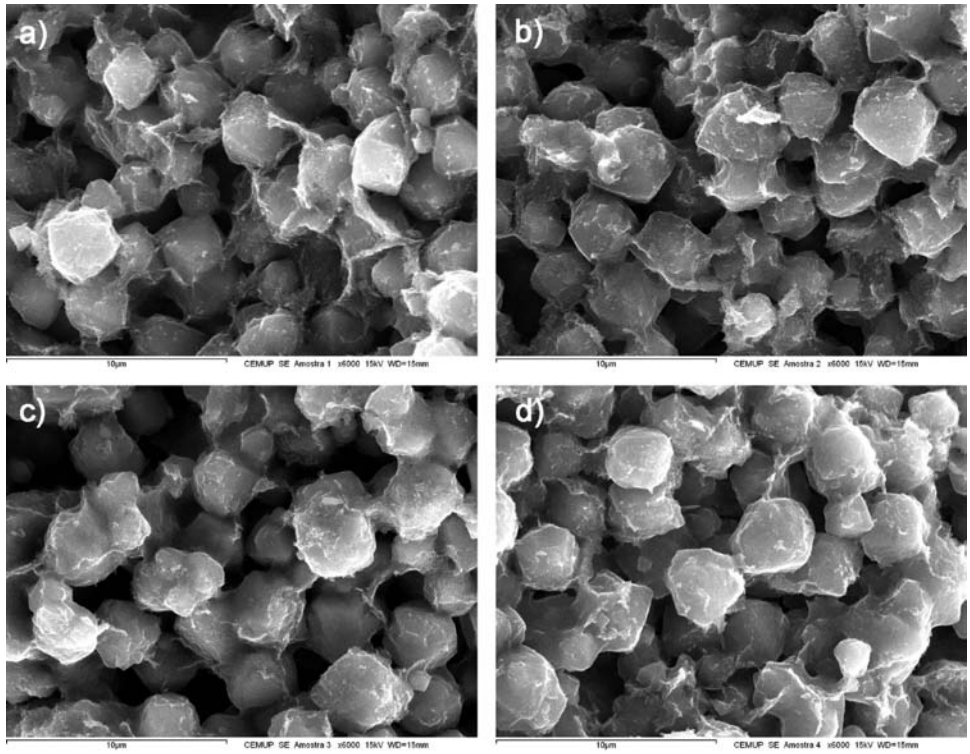

Figure 1. Scanning electron microscopy (SEM) image of zeolite 13X (a) and ion-exchanged zeolites 13X-Li (b), 13X-Ba (c), and 13X-Ca (d).

the samples of zeolite 13X and of the three ion-exchanged samples (13X-Li, 13X-Ba, and 13X-Ca) are shown in Figure 1. The dimensions of the crystals determined by SEM are ~3 μm. It was observed that the crystals were not damaged or destroyed after the ion exchange.

Energy dispersive X-ray (EDX) analyses of the four zeolite samples (13X, 13X-Li, 13X-Ba, and 13X-Ca) were performed to observe the effects of ion exchange. The EDX patterns are shown in Figure 2. All the exchanged samples show a significant reduction of the amount of sodium in the zeolite structure when compared to the original sample.

For the scale-up sample of zeolite 13X-Ca, the obtained evolution of Na^+ concentration for each exchange was determined by atomic absorption (Figure 3). It is observed that the equilibrium is reached after ~250 min. The determined Na^+ concentrations in solution are, respectively, (11.4, 3.7, 1.5, and 0.9) $g \cdot L^{-1}$ at the end of each exchange. The ion exchange results in a final total concentration of 0.076 $g_{calcium}/g_{material}$ on the structure of the modified zeolite material.

3.2. Nitrogen Adsorption on Ion-Exchanged Zeolites. Breakthrough curves of nitrogen in all the zeolites 13X, 13X-Li, 13X-Ba, and 13X-Ca are reported in Figure 4. Two different concentrations of nitrogen were employed to determine the difference in capacity between high and low pressure. This difference in loading is related to the effective capacity in a PSA unit. Using these breakthrough curves, the amount of nitrogen adsorbed for the four samples was determined (Table 3).

The breakthrough curves were also employed to determine diffusion parameters in the different samples. In previous studies, it was reported that diffusion within zeolite extrudates of 13X was controlled by macropore diffusion.[29] However, the diameter of zeolite crystals in this sample is much larger as well as the pore network of the binder. For these reasons, we have observed that the diffusion mechanism is controlled within the crystals of the zeolite. The crystal diffusivities in the four zeolite samples were also determined for nitrogen at (303 and 323) K using the breakthrough curves with 1.0 % N_2 balanced in helium. The results are reported in Table 3. No significant variations were observed in the shape of the curves indicating that the prepared samples do not present any additional resistance for diffusion. For the more concentrated experiments (Figures 4c and 4d), the stronger nonlinearity of the 13X-Ca sample results in a steeper concentration front. In the Appendix, Table A.1 shows the contributions of mass transfer resistances.

Table 3 shows a largest crystal diffusivity value at both temperatures for zeolite 13X-Ba, followed by zeolites 13X, 13X-Li, and 13X-Ca. The nitrogen crystal diffusivities (D_c) for the zeolite 13X published in the literature[36,37] are ($3.00 \cdot 10^{-8}$ and $4.00 \cdot 10^{-8}$) $m^2 \cdot s^{-1}$ at (301 and 323) K, respectively. This means that the nitrogen crystal diffusivities obtained in this study are 4 orders of magnitude lower. However, the reported values were determined by microscopic methods (N. M. R.), and it is well known that important differences may be obtained in comparing values obtained by micro- and macroscopic methods.[38] Table 3 also shows an increase of the adsorption capacity of all the ion-exchanged samples of zeolite 13X for nitrogen, with the exception of zeolite 13X-Li. The difference of useful capacities between high and low pressure of zeolites 13X-Ba and 13X-Ca for nitrogen relative to the zeolite 13X is ~1.37 and ~2.24, respectively. Therefore, since the resistance of diffusion in all zeolite samples is similar, the ion exchange of zeolite 13X with Ba^{2+} and Ca^{2+} will favor the nitrogen adsorption for separations of this gas in a PSA unit. This result is not contradictory with air separation processes (where 13X-Li is employed).[39] The main difference is that in this particular application the partial pressure of N_2 is much smaller, and 13X-Li isotherms (less steep) present lower loading at low partial pressures.

From these experiments, we have determined that the adsorbent with a higher operating capacity for a PSA unit is the 13X-Ca sample, and further studies were performed on this sample.

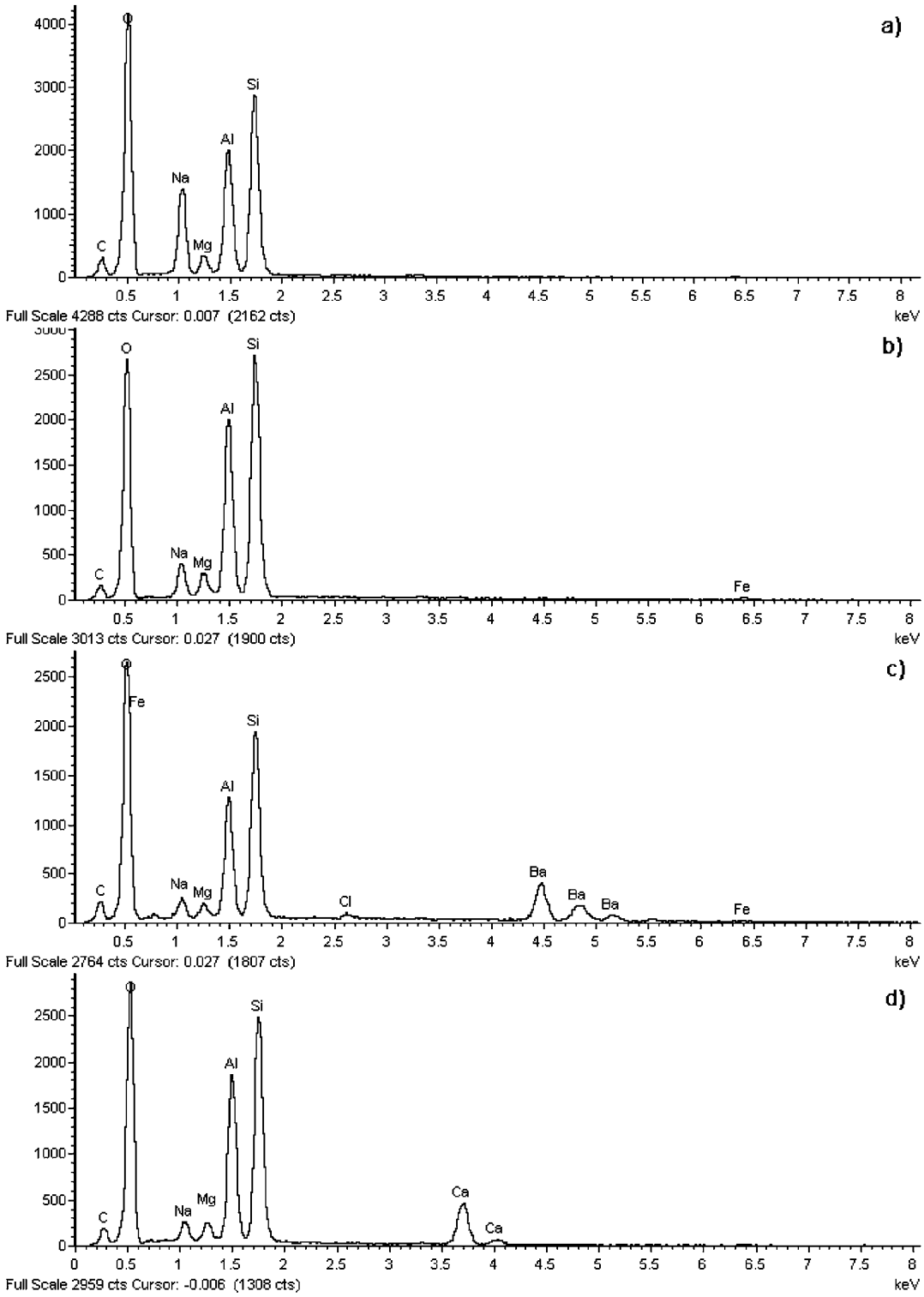

Figure 2. Energy dispersive X-ray (EDX) pattern of zeolite 13X (a) and ion-exchanged zeolites 13X-Li (b), 13X-Ba (c), and 13X-Ca (d).

3.3. Adsorption Kinetics of CO_2, CH_4, CO, and H_2. The breakthrough curves of CO_2, CH_4, CO, and H_2 for the exchanged zeolite 13X sample with the highest performance for nitrogen at (303 and 323) K are reported in Figure 5. The dispersive effects are more evident in the breakthrough curves of methane and carbon monoxide than for hydrogen or carbon dioxide. However, the outlet front of CO_2 takes more time to completely leave the column. Therefore, it is expected that carbon dioxide has a slower diffusion than the other gases.

The reciprocal time constant for crystal diffusion (D_c/r_c^2) was determined for CO_2, CH_4, CO, and H_2 in zeolite 13X-Ca at both temperatures, and the results are reported in Table 4. According to the analysis of the derivative of each breakthrough curve, the most relevant dispersive mechanism is the axial dispersion term, and the micropore diffusivity is the controlling mechanism for all gases (comparing the contributions of the three mass transfer resistances). In Table A.2 of the Appendix, a comparison of the contributions of mass transfer resistances is reported.

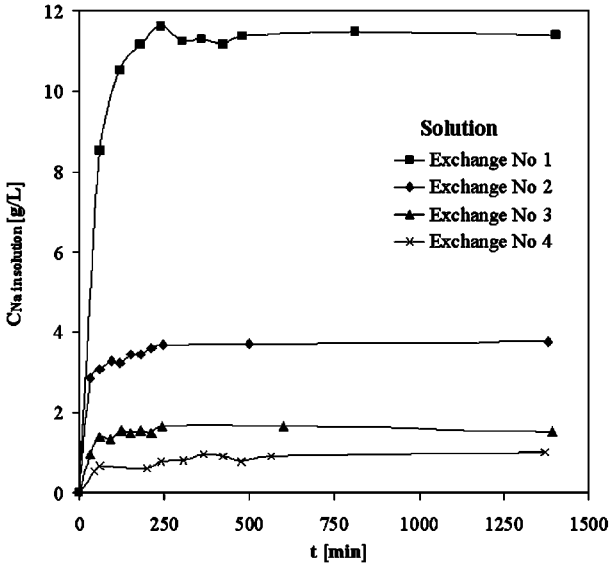

Figure 3. Concentration history of the Na^+ cation exchange in zeolite 13X using 400 mL of 1 N Ca^{2+} solutions and 80 g of zeolite: exchange nos.: -■-, 1; -◆-, 2; -▲-, 3; and -×-, 4.

However, changing the correlation of the axial dispersion coefficient, the variations in the estimation of the crystal diffusivity values are lower than 10 % (see Table A.3 in the Appendix). It was observed that hydrogen has the fastest micropore diffusion in the zeolite 13X-Ca followed by nitrogen, methane, carbon monoxide, and finally carbon dioxide. Diffusion of CO and CO_2 is much slower than the other gases due to stronger electrostatic interactions with the zeolite framework. In the case of methane and nitrogen, the interactions are less strong and thus diffusion is controlled by the kinetic diameter of the molecules (3.6 Å for N_2 and 3.8 Å for CH_4). The crystal diffusivities (D_c) published in the literature[36,37] are $3.92 \cdot 10^{-15}$ $m^2 \cdot s^{-1}$ (301 K) and $5.35 \cdot 10^{-15}$ $m^2 \cdot s^{-1}$ (323 K) for carbon dioxide and $3.00 \cdot 10^{-8}$ $m^2 \cdot s^{-1}$ (301 K) and $3.30 \cdot 10^{-8}$ $m^2 \cdot s^{-1}$ (323 K) for methane. The carbon dioxide crystal diffusivities obtained in this study are in the same order of magnitude as the published results. However, for methane, the crystal diffusivities obtained are 6 orders of magnitude lower than the published results.

3.4. Adsorption Equilibrium of N_2, CO_2, CH_4, CO, and H_2. Adsorption equilibria of nitrogen on ion exchanged zeolite 13X-Ca was studied at (303 and 323) K over the pressure range (0 to 7) bar. Figure 6 shows the absolute amount of nitrogen adsorbed on zeolite 13X-Ca and compared to data reported in the literature.[40−43] Dantas et al. (2008)[41] reported the adsorption equilibrium of nitrogen at 301 K on the commercial zeolite 13X used for this study. At 303 K and 7 bar, the amount adsorbed of nitrogen on the zeolites 13X and 13X-Ca is (1.47,[40] 1.16,[42] 1.18,[43] and 1.27) $mol \cdot kg^{-1}$, respectively. For the same temperature at 1 bar, the N_2 amount adsorbed on zeolites 13X is

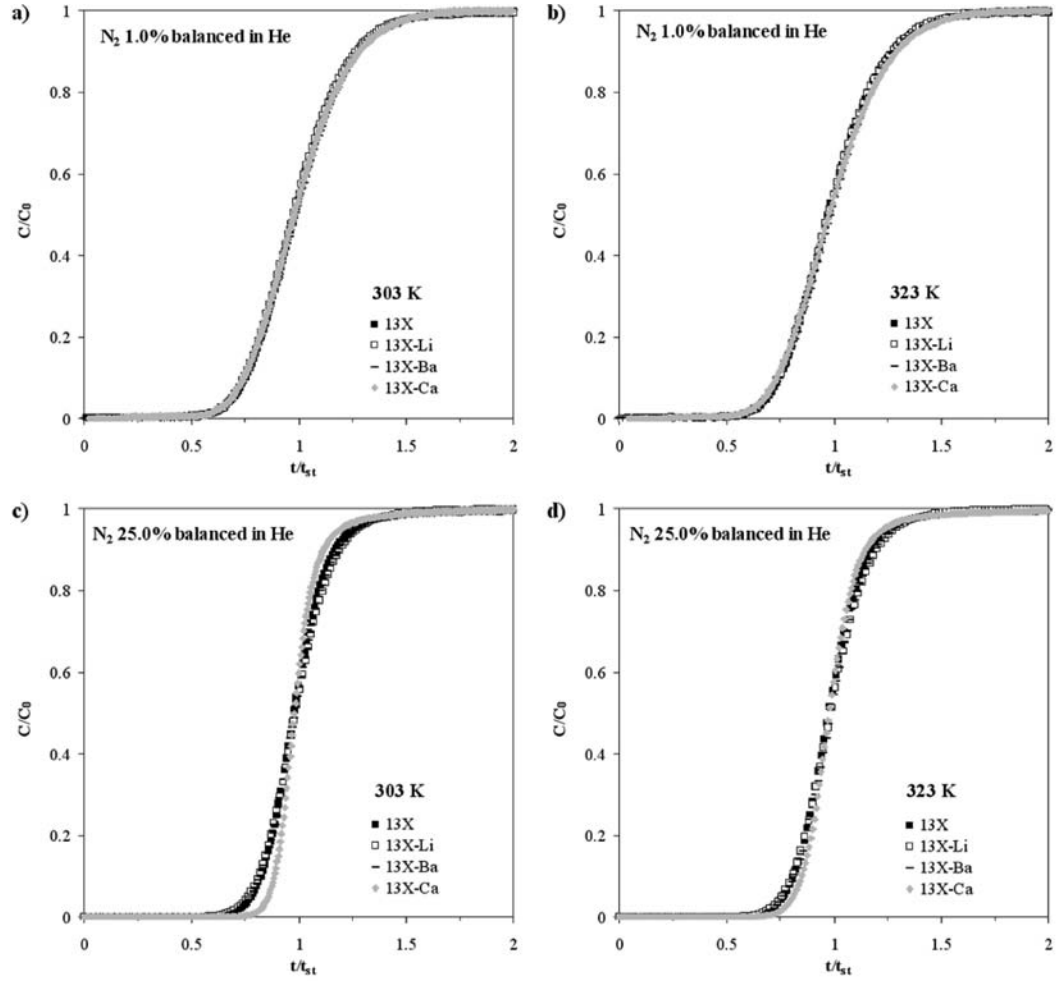

Figure 4. Breakthrough curves of 0.01 bar of N_2 balanced in He [(a) 303 K and (b) 323 K] and 0.25 bar of N_2 balanced in He [(c) 303 K and (d) 323 K] on the ■, zeolite 13X; □, 13X-Li; −, 13X-Ba; and ◆, 13X-Ca; experimental conditions and results reported in Tables 1 and 3.

Table 3. Breakthrough Experimental Results Obtained for Nitrogen (Mixtures of 1.0 % or 25.0 % of N_2 Balanced in He) in Zeolites 13X, 13X-Li, 13X-Ba, and 13X-Ca at (303 and 323) K and 1 bar of Total Pressure

p_{N_2}[bar]	zeolite	13X		13X-Li		13X-Ba		13X-Ca	
	temperature [K]	303	323	303	323	303	323	303	323
0.01	μ_1 [s]	110.9	75.7	80.0	57.5	131.1	85.4	287.3	141.1
	σ^2 [s^2]	587.7	327.0	421.6	250.6	771.7	387.2	3097	893.0
	$u_0 \cdot 10^2$ [m·s^{-1}]	5.46	5.82	5.43	5.78	5.48	5.84	5.47	5.83
	$u_i \cdot 10^2$ [m·s^{-1}]	2.16	2.30	2.15	2.30	2.16	2.31	2.16	2.30
	$q \cdot 10^3$ [mol·kg^{-1}]	2.936	1.947	2.753	1.926	3.758	2.394	9.026	4.145
	K_H [mol·kg^{-1}·bar^{-1}]	0.290	0.193	0.272	0.188	0.371	0.237	0.914	0.440
	$D_c/r_c^2 \cdot 10^2$ [s^{-1}][a]	4.07	4.43	3.74	4.05	4.73	5.24	3.48	4.57
	$(D_c\|_{\text{exchanged 13X}})/(D_c\|_{13X})$ [-]	1.00	1.00	0.920	0.916	1.16	1.18	0.85	1.03
0.25	μ_1 [s]	107.7	74.4	75.5	56.1	121.9	82.1	199.7	121.2
	$q \cdot 10^2$ [mol·kg^{-1}]	7.890	5.357	6.710	4.914	10.81	7.173	17.95	10.78
	$\Delta q \cdot 10^2$ [mol·kg^{-1}]	7.596	5.162	6.435	4.721	10.43	6.934	17.05	10.37
	$(\Delta q\|_{\text{exchanged 13X}})/(\Delta q\|_{13X})$ [-]	1.00	1.00	0.847	0.915	1.37	1.34	2.24	2.00

At 303 K: $Q = 6.44 \cdot 10^{-7}$ m^3·s^{-1}; $C_0 = 0.402$ mol·m^{-3}; $D_{ax} = 3.38 \cdot 10^{-5}$ m^2·s^{-1}; $D_m = 7.18 \cdot 10^{-5}$ m^2·s^{-1}; $D_p = 3.59 \cdot 10^{-5}$ m^2·s^{-1}; $k_f = 0.1001$ m·s^{-1}
At 323 K: $Q = 6.87 \cdot 10^{-7}$ m^3·s^{-1}; $C_0 = 0.377$ mol·m^{-3}; $D_{ax} = 3.73 \cdot 10^{-5}$ m^2·s^{-1}; $D_m = 7.99 \cdot 10^{-5}$ m^2·s^{-1}; $D_p = 3.99 \cdot 10^{-5}$ m^2·s^{-1}; $k_f = 0.1109$ m·s^{-1}

[a] Estimated using a tortuosity factor, $\tau_p = 2$; $\Delta q = (q|_{0.25\text{bar}} - q|_{0.01\text{bar}})$.

Table 4. Breakthrough Experimental Results Obtained for Carbon Dioxide, Methane, Carbon Monoxide, and Hydrogen in Ion Exchanged Zeolite 13X-Ca at (303 and 323) K and 1 bar of Total Pressure

adsorbate	CO_2		CH_4		CO		H_2[a]	
temperature [K]	303	323	303	323	303	323	303	323
μ_1 [s]	11864	8051	214.7	119.1	1657	713.7	11.94	10.38
σ^2 [s^2]	8374750	4011770	3490	1218	166236	34326	12.65	9.18
$D_m \cdot 10^5$ [m^2·s^{-1}]	5.98	6.66	6.98	7.77	7.30	8.12	16.2	18.0
$D_{ax} \cdot 10^5$ [m^2·s^{-1}]	2.92	3.22	3.30	3.64	3.42	3.78	6.83	7.56
$D_p \cdot 10^5$ [m^2·s^{-1}]	2.99	3.33	3.49	3.88	3.65	4.06	8.11	9.02
k_f [m·s^{-1}]	0.0841	0.0933	0.0972	0.1077	0.1015	0.1125	0.2179	0.2415
$K_H(\mu_1)$ [mol·kg^{-1}·bar^{-1}]	67.4	45.6	1.19	0.650	9.30	4.00	0.0179	0.0142
K_H(fitting) [mol·kg^{-1}·bar^{-1}]	53.5	19.9	1.77	0.72	4.86	3.16	0.0317	0.0237
$D_c/r_c^2 \cdot 10^2$ [s^{-1}][b]	0.0544	0.0753	1.85	2.59	0.491	0.848	12.0	14.3
At 303 K: $Q = 6.38 \cdot 10^{-7}$ m^3·s^{-1}; $C_0 = 0.201$ mol·m^{-3} ($C_0 = 40.22$ mol·m^{-3} for H_2); $u_0 = 5.30 \cdot 10^{-2}$ m·s^{-1} ($u_0 = 5.47 \cdot 10^{-2}$ m·s^{-1} for H_2); $u_i = 2.12 \cdot 10^{-2}$ m·s^{-1} ($u_i = 2.16 \cdot 10^{-2}$ m·s^{-1} for H_2).								
At 323 K: $Q = 6.80 \cdot 10^{-7}$ m^3·s^{-1}; $C_0 = 0.189$ mol·m^{-3} ($C_0 = 37.73$ mol·m^{-3} for H_2); $u_0 = 5.65 \cdot 10^{-2}$ m·s^{-1} ($u_0 = 5.83 \cdot 10^{-2}$ m·s^{-1} for H_2); $u_i = 2.26 \cdot 10^{-2}$ m·s^{-1} ($u_i = 2.30 \cdot 10^{-2}$ m·s^{-1} for H_2)								

[a] The adsorbate partial pressure is 1 bar for H_2; for the other gases it is 0.005 bar. [b] Estimated using a tortuosity factor, $\tau_p = 2$.

Table 5. Virial Adsorption Isotherm Fitting Parameters of N_2, CO_2, CH_4, CO, and H_2 for the Ion Exchanged Zeolite 13X-Ca at (303 to 323) K

adsorbate	K_∞ [mol·kg^{-1}·bar^{-1}]	$(-\Delta H)$ [kJ·mol^{-1}]	$A_0 \cdot 10^{-5}$ [m^2·mol^{-1}]	$A_1 \cdot 10^{-6}$ [m^{2}K·mol^{-1}]	$B_0 \cdot 10^{-11}$ [m^4·mol^{-2}]	$B_1 \cdot 10^{-11}$ [m^{4}K·mol^{-2}]
N_2	$1.19 \cdot 10^{-3}$	16.52	48.0	−1222	−51.09	14926
CO_2	$6.16 \cdot 10^{-6}$	40.25	0.028	−4.663	0.010	308.5
CH_4	$8.89 \cdot 10^{-7}$	36.54	4.49	94.67	−14.46	3796
CO	$4.81 \cdot 10^{-3}$	17.43	27.2	−468.2	−16.01	3979
H_2	$2.93 \cdot 10^{-4}$	11.80	12.24	0.401	−56.71	4200

[0.288,[40] 0.258 (at 301 K),[41] 0.258,[42] and 0.261[43]] mol·kg^{-1} and on 13X-Ca is 0.447 mol·kg^{-1}. Figure 6 shows the increase of the nonlinearity of the N_2 isotherms on zeolite 13X-Ca. It is also possible to observe that the N_2 adsorption capacity on zeolite 13X-Ca is larger than on the original zeolite 13X below ~3 bar, which is usually within the nitrogen partial pressure range of the SMR off-gases. Besides, the differential N_2 loading between the high and low pressures of the PSA process is enlarged. Therefore the second layer (zeolite) can be smaller, and the productivity of the PSA process for hydrogen purification is improved.

Also, adsorption equilibria of H_2, CO_2, CH_4, and CO on the ion exchanged zeolite 13X-Ca were studied at the same temperature and pressure ranges (Figure 7). The amount of hydrogen adsorbed on zeolite 13X-Ca is small, and the linearity of the isotherm is observed. On the other hand, the CO_2 isotherm on the ion exchanged zeolite 13X-Ca shows a high steepness, eventually due to the high charge density of the calcium cation, with an amount adsorbed of ~7.5 mol·kg^{-1} at 303 K and 7 bar. This high steepness results in an unfavorable desorption of carbon dioxide from the zeolite with a high heat of desorption. Therefore, it is important that no CO_2 passes through the first layer (activated carbon) to the second layer (zeolite) of the PSA column. The CH_4 and CO adsorption capacities of this material at 303 K and 7 bar are approximately the same, i.e., ~2 mol·kg^{-1}.

All adsorption data on the ion exchanged zeolite 13X-Ca at (303 to 323) K were fitted employing the virial isotherm equation, which describes the adsorption isotherms in the whole temperature and pressure ranges studied. The virial parameters are detailed in Table 5. For that, the temperature dependence of the virial coefficients was truncated at the second term. Figures 6 and 7 shows a good fitting for all the compounds (N_2, CO_2, CH_4, CO, and H_2) over the whole pressure and temperature ranges studied. It was found that the isosteric heats of adsorption obtained through the virial isotherm model are in

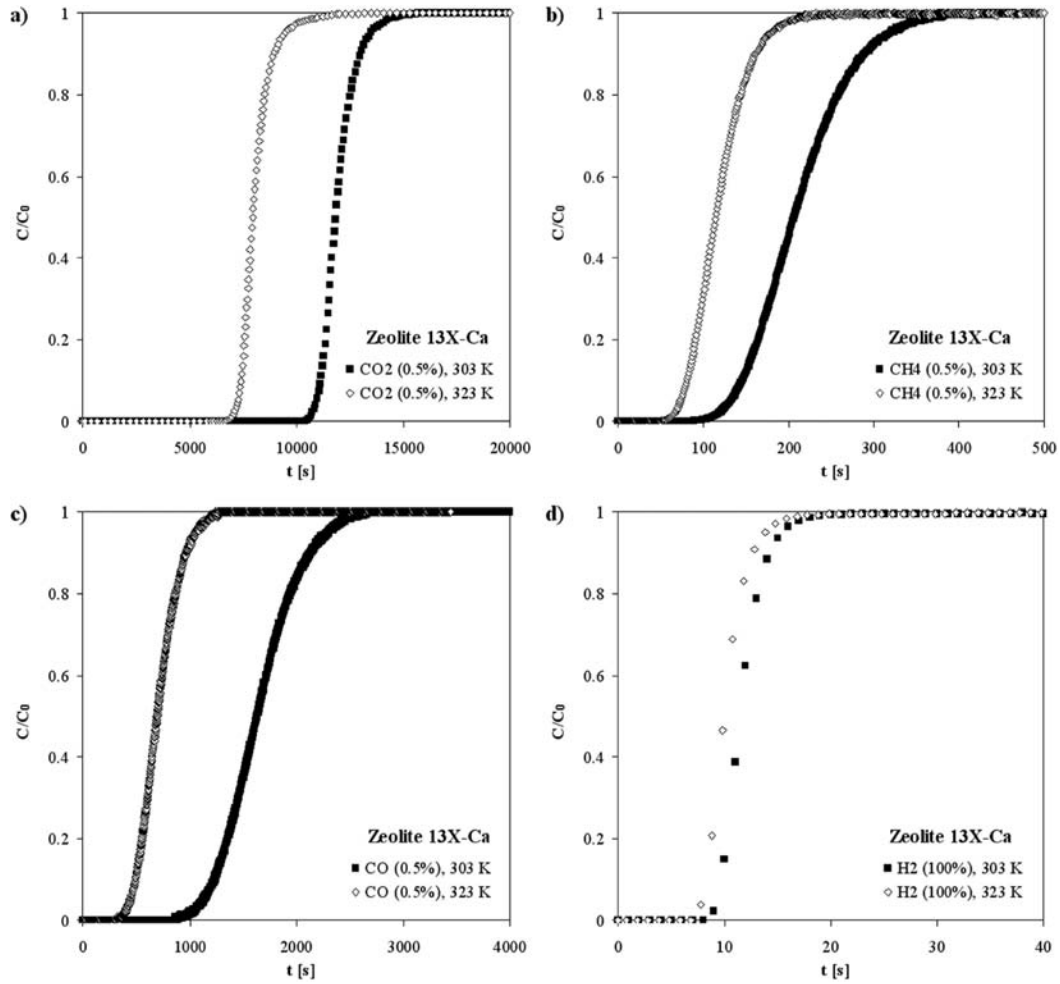

Figure 5. Diluted breakthrough curves (0.005 bar of adsorbate balanced in He) of CO_2 (a), CH_4 (b), and CO (c) and breakthrough of pure H_2 (d) on zeolite 13X-Ca at (303 and 323) K (■, ◇); experimental conditions and results reported in Tables 1 and 4.

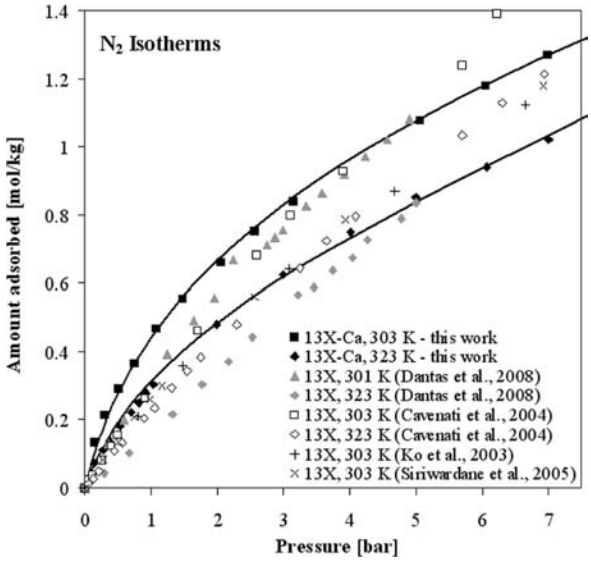

Figure 6. Amount adsorbed of N_2 on zeolite 13X-Ca: experimental points at (303 and 323) K (■,◆) and —, virial isotherm fitting; comparison to published results of N_2 amount adsorbed on the studied sample of zeolite 13X (▲,◆) and other samples of zeolite 13X (□,◇,+,×).

agreement with the values calculated using the Clausius−Clapeyron equation (Figure 8).

When the Henry constants obtained from the first moment $K_H(\mu_1)$ are compared with the values obtained by fitting equilibrium data to the virial isotherm expression K_H(fitting), it can be concluded that these results have the same order of magnitude.

4. Conclusions

The adsorption equilibrium of each pure gas employed in an equilibrium-based separation process is the fundamental property to be measured since it determines the maximum efficiency of the PSA unit. Thus, it is important to report a complete study of the adsorption equilibrium of the SMR off-gases (CO_2, H_2, CH_4, CO, and N_2) on different zeolites, such as the zeolite 13X and the ion exchanged samples of zeolites 13X-Li, 13X-Ba, and 13X-Ca.

There ion exchanged zeolite samples (13X-Li, 13X-Ba, and 13X-Ca) were prepared with Li^+, Ba^{2+}, and Ca^{2+} starting from a commercial zeolite 13X. The zeolite 13X and the exchanged zeolite samples were characterized by SEM for the study of the morphology of the particles and by EDX for identification and quantification of the elemental composition. It was concluded that the crystals were not damaged or destroyed after performing the ion exchange, and also a final total concentration of 0.076 $g_{calcium}/g_{material}$ on the structure of the modified zeolite 13X-Ca was achieved.

To study the adsorption equilibrium of nitrogen, breakthrough curves at (303 and 323) K were performed on all zeolite samples

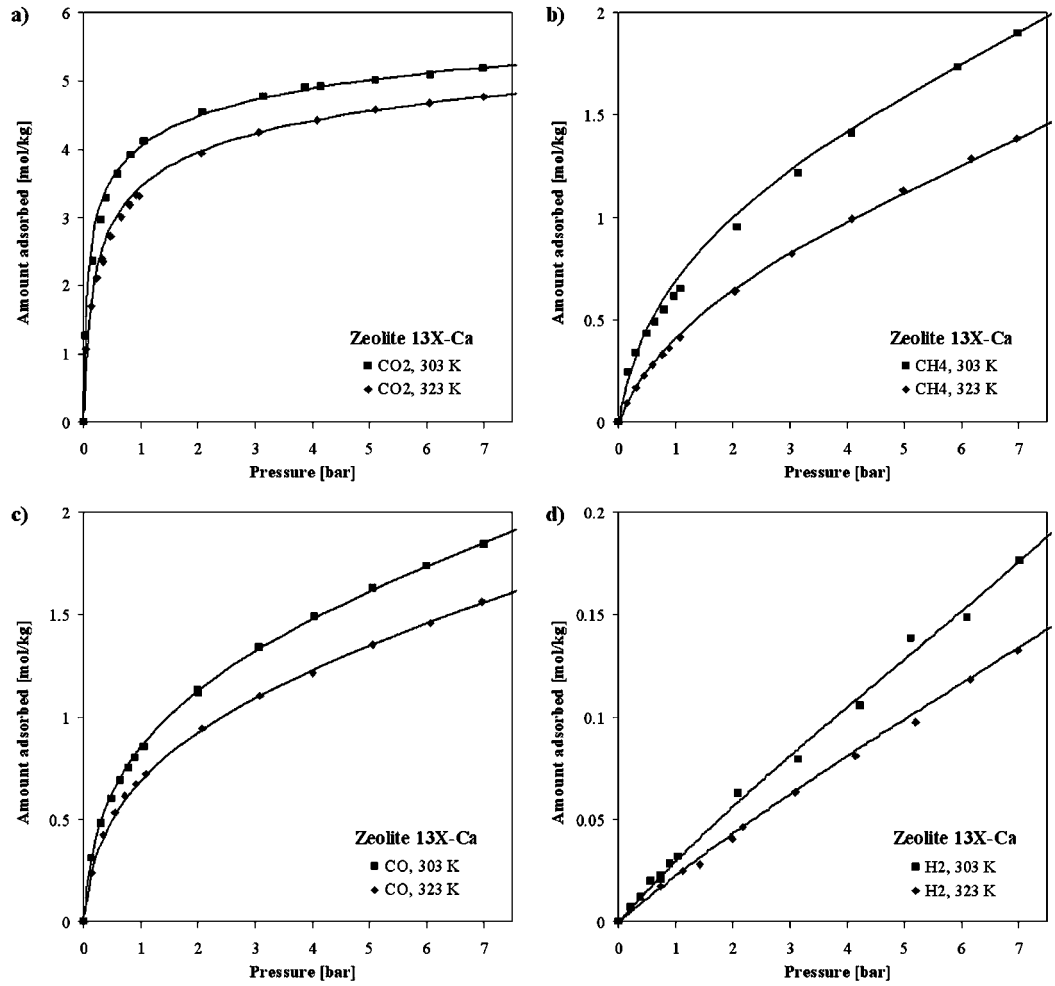

Figure 7. Amount adsorbed of CO_2 (a), CH_4 (b), CO (c), and H_2 (d) on zeolite 13X-Ca: experimental points at (303 and 323) K (■,◆) and —, virial isotherm fitting.

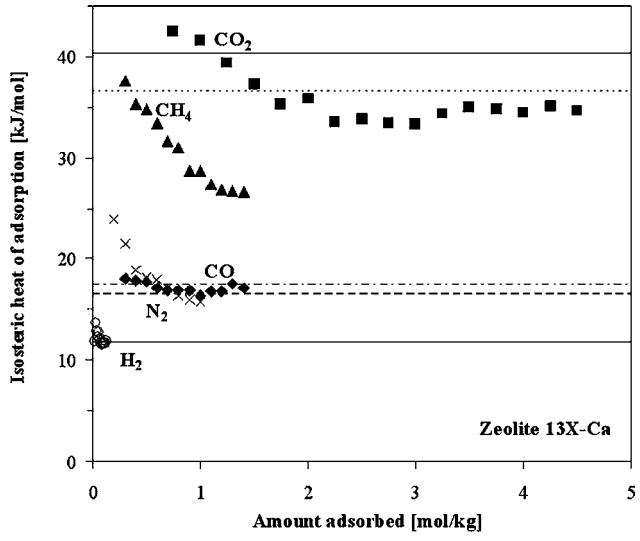

Figure 8. Isosteric heats of adsorption of ■, CO_2; ▲, CH_4; ◆, CO; ×, N_2; and ○, H_2 on zeolite 13X-Ca as a function of equilibrium pressure in the temperature range of (303 to 323) K; lines are the values obtained through the virial model.

(13X, 13X-Li, 13X-Ba, and 13X-Ca) with two pure nitrogen mixtures: (1) N_2 partial pressure of 0.01 bar and (2) N_2 partial pressure of 0.25 bar. The N_2 crystal diffusivity was estimated using the breakthrough experiments of 1.0 % nitrogen balanced in helium. It was verified that the crystal diffusivities of all samples are of the same order of magnitude, and they are approximately the same. At 303 K, the ratio of the difference in capacity between high and low pressure [(0.25 and 0.01) bar] of the zeolites 13X-Ba and 13X is ~1.4, for zeolites 13X-Ca and 13X is ~2.2, and for zeolites 13X-Li and 13X is ~0.8. So, the use of zeolite 13X exchanged with barium and calcium will improve the nitrogen adsorption for separations of this gas. The transport kinetics of carbon dioxide, methane, carbon monoxide, and hydrogen was also studied in the zeolite 13X-Ca by breakthrough curves at (303 and 323) K. The crystal diffusivities of N_2, CO_2, CH_4, CO, and H_2 in the zeolite 13X-Ca differ by 2 orders of magnitude having the following order from the slowest to the fastest species: $CO_2 < CO < CH_4 < N_2 < H_2$. It was also concluded that the axial dispersion term is the most relevant dispersive mechanism, and the contributions of film and macropore mass transfer resistances to the total dispersion were negligible.

Adsorption equilibria of nitrogen, carbon dioxide, methane, carbon monoxide, and hydrogen are reported for zeolite 13X-Ca at (303 and 323) K. The nitrogen adsorption capacity of the ion exchanged zeolite 13X-Ca in the pressure range of (0 to 3) bar is higher than the adsorption capacity of the original zeolite 13X (at 1 bar it increases 36 %).

It can be concluded that the capacity toward nitrogen of the zeolite 13X can be enhanced by ion exchange of the zeolite

material with Ca^{2+}. Therefore, the ion exchanged zeolite (13X-Ca) will provide a higher productivity to the layered PSA process applied for SMR off-gases separation.

Nomenclature

A	Virial coefficients ($m^2 \cdot mol^{-1}$)
B	Virial coefficients ($m^4 \cdot mol^{-2}$)
C	Concentration ($mol \cdot m^{-3}$)
C_0	Concentration of saturation ($mol \cdot m^{-3}$)
D_{ax}	Axial dispersion coefficient ($m^2 \cdot s^{-1}$)
D_c	Crystal diffusivity ($m^2 \cdot s^{-1}$)
D_{ij}	Binary molecular diffusivity ($m^2 \cdot s^{-1}$)
D_k	Knudsen diffusivity ($m^2 \cdot s^{-1}$)
D_m	Molecular diffusivity ($m^2 \cdot s^{-1}$)
D_p	Macropore diffusivity ($m^2 \cdot s^{-1}$)
k_f	Film mass transfer coefficient ($m \cdot s^{-1}$)
K_H	Henry constant ($mol \cdot kg^{-1} \cdot bar^{-1}$)
K_∞	Adsorption constant at infinite temperature ($mol \cdot kg^{-1} \cdot bar^{-1}$)
L	Column length (m)
m_s	Mass of adsorbent (kg)
M_W	Molecular weight of the gas ($kg \cdot mol^{-1}$)
N	Number of points of each isotherm
p_{N_2}	Nitrogen partial pressure (Pa)
P	Pressure (Pa)
P_{cal}	Calculated partial pressure (Pa)
P_{exp}	Experimental partial pressure (Pa)
q	Absolute adsorbed phase concentration ($mol \cdot kg^{-1}$)
Q	Flow rate ($m^3 \cdot s^{-1}$)
r_c	Crystal radius (m)
r_p	Mean pore radius (m)
R_g	Universal gas constant ($J \cdot mol^{-1} \cdot K^{-1}$)
R_p	Radius of the adsorbent extrudates (m)
Re	Reynolds number
S	Adsorbent specific area ($m^2 \cdot kg^{-1}$)
Sc	Schmidt number
Sh	Sherwood number
t	Time (s)
T	Temperature (K)
u_0	Superficial velocity ($m \cdot s^{-1}$)
u_i	Interstitial velocity ($m \cdot s^{-1}$)
V_c	Volume of the cell where the adsorbent is located (m^3)
V_s	Volume of the solid adsorbent (m^3)
w	Error parameter between 0 and 1
y_i	Molar fraction of component i

Greek Letters

Δm	Difference of weight between two measurements (kg)
Δq	Difference of absolute adsorbed phase concentration for the partial pressure range (0.01 to 0.25) bar ($mol \cdot kg^{-1}$)
$(-\Delta H)$	Isosteric heat of adsorption ($kJ \cdot mol^{-1}$)
ε	Bed porosity
ε_p	Particle porosity
μ	Gas viscosity ($Pa \cdot s$)
μ_1	First moment (s)
ρ_g	Density of the gas phase ($kg \cdot m^{-3}$)
$\rho_/$	Density of the adsorbed phase ($kg \cdot m^{-3}$)
ρ_p	Adsorbent (particle) density ($kg \cdot m^{-3}$)
ρ_s	Solid density ($kg \cdot m^{-3}$)
σ^2	Variance (s^2)
τ_p	Pore tortuosity

Appendix

According to the analysis of the derivative of each breakthrough curve, the contributions of mass transfer resistances were determined. Table A.1 shows the contributions of mass transfer resistances for the N_2 breakthrough experiments in zeolites 13X, 13X-Li, 13X-Ba, and 13X-Ca. In Table A.2, the contributions of mass transfer resistances for all gases (CO_2, H_2, CH_4, CO, and N_2) in zeolite 13X-Ca are reported.

The crystal diffusivities were also studied varying the tortuosity and the axial dispersion coefficient correlation. Changing the tortuosity from 2 to 6, the estimation of the macropore diffusivity will be slightly affected. The values are in the same order of magnitude, and this leads to a maximum of ~40 % variation in the crystal diffusivity coefficients (Table A.1). On the other hand, changing the correlation of the axial dispersion coefficient to $D_{ax}^* = \varepsilon D_m + 0.35 R_p u_i$, the variations in the estimation of the crystal diffusivity values are less significant (maximum variation of ~10 %). Once again, the values D_{ax}^* and D_{ax} are in the same order of magnitude resulting in similar crystal diffusivity coefficients (Table A.3).

Table A.1. Contributions of the Axial Dispersion Term, Film Mass Transfer Term, Pore Resistance Term, and Crystal Resistance Term for N_2 in Zeolites 13X, 13X-Li, 13X-Ba, and 13X-Ca at (303 and 323) K and 1 bar of Total Pressure

		term contribution [%]			
adsorbent	temp. [K]	axial disp.	film M.T.	pore res.	crystal. res.
3X	303	39.7	1.3	2.0	57.0
	323	34.7	1.0	1.5	62.8
13X-Li	303	35.6	1.1	1.6	61.7
	323	31.4	0.9	1.3	66.4
13X-Ba	303	50.1	1.7	3.2	45.0
	323	44.3	1.4	2.5	51.9
13X-Ca	303	60.1	2.2	3.4	34.3
	323	52.0	1.7	2.7	43.6

$$\frac{\sigma^2}{2\mu_1^2} = \begin{Bmatrix}\text{Axial}\\ \text{Disp.}\end{Bmatrix} + \left(\frac{u_i}{L}\right)\left(\frac{\varepsilon}{1-\varepsilon}\right)\left(\begin{Bmatrix}\text{film}\\ \text{M.T.}\end{Bmatrix} + \begin{Bmatrix}\text{pore}\\ \text{res.}\end{Bmatrix} + \begin{Bmatrix}\text{crystal}\\ \text{resist.}\end{Bmatrix}\right)\left(1 + \frac{\varepsilon_p}{(1-\varepsilon_p)K_H \rho_p R_g T}\right)^{-2}$$

Table A.2. Contributions of the Axial Dispersion Term, Film Mass Transfer Term, Pore Resistance Term, and Crystal Resistance Term for CO_2, H_2, CH_4, CO, and N_2 in Zeolite 13X-Ca at (303 and 323) K and 1 bar of Total Pressure

		term contribution [%]			
adsorbate	temp. [K]	axial disp.	film M.T.	pore res.	crystal. res.
CO_2	303	57.9	3.0	4.7	34.4
	323	57.6	2.8	4.3	35.3
H_2	303	51.25	0.10	0.15	48.50
	323	55.50	0.08	0.12	44.30
CH_4	303	51.5	2.0	3.0	43.5
	323	47.1	1.6	2.5	48.8
CO	303	66.8	2.4	3.8	27.0
	323	62.1	2.1	3.2	32.6
N_2	303	60.1	2.2	3.4	34.3
	323	52.0	1.7	2.7	43.6

$$\frac{\sigma^2}{2\mu_1^2} = \begin{Bmatrix}\text{Axial}\\ \text{Disp.}\end{Bmatrix} + \left(\frac{u_i}{L}\right)\left(\frac{\varepsilon}{1-\varepsilon}\right)\left(\begin{Bmatrix}\text{film}\\ \text{M.T.}\end{Bmatrix} + \begin{Bmatrix}\text{pore}\\ \text{res.}\end{Bmatrix} + \begin{Bmatrix}\text{crystal}\\ \text{resist.}\end{Bmatrix}\right)\left(1 + \frac{\varepsilon_p}{(1-\varepsilon_p)K_H \rho_p R_g T}\right)^{-2}$$

Table A.3. Breakthrough Experimental Results Obtained for Carbon Dioxide, Methane, Carbon Monoxide, and Hydrogen in Ion Exchanged Zeolite 13X-Ca at (303 and 323) K and 1 bar of Total Pressure Changing the Tortuosity Factor or the Axial Dispersion Correlation

adsorbate	CO_2		CH_4		CO		H_2[a]	
temperature [K]	303	323	303	323	303	323	303	323
μ_1 [s]	11864	8051	214.7	119.1	1657	713.7	11.94	10.38
σ^2 [s^2]	8374750	4011770	3490	1218	166236	34326	12.65	9.18
$D_m \cdot 10^5$ [m^2·s^{-1}]	5.98	6.66	6.98	7.77	7.30	8.12	16.2	18.0
changing the tortuosity from 2 to 6								
$D_{ax} \cdot 10^5$ [m^2·s^{-1}]	2.92	3.22	3.30	3.64	3.42	3.78	6.83	7.56
$D_p(\tau_p = 2) \cdot 10^5$ [m^2·s^{-1}]	2.99	3.33	3.49	3.88	3.65	4.06	8.11	9.02
$D_p(\tau_p = 6) \cdot 10^5$ [m·s^{-1}]	1.00	1.11	1.16	1.29	1.22	1.35	2.70	3.01
k_f [m·s^{-1}]	0.0841	0.0933	0.0972	0.1077	0.1015	0.1125	0.2179	0.2415
$K_H(\mu_1)$ [mol·kg^{-1}·bar^{-1}]	67.4	45.6	1.19	0.650	9.30	4.00	0.0179	0.0142
K_H(fitting) [mol·kg^{-1}·bar^{-1}]	53.5	19.9	1.77	0.72	4.86	3.16	0.0317	0.0237
$D_c/r_c^2(\tau_p = 2) \cdot 10^2$ [s^{-1}]	0.0544	0.0753	1.85	2.59	0.491	0.848	12.0	14.3
$D_c/r_c^2(\tau_p = 6) \cdot 10^2$ [s^{-1}]	0.0749	0.0998	2.15	2.89	0.681	1.06	12.1	14.4
changing the correlation of the axial dispersion coefficient to $D_{ax}{}^a = \varepsilon D_m + 0.35 R_p u_i$								
$D_{ax} \cdot 10^5$ [m^2·s^{-1}]	2.92	3.22	3.30	3.64	3.42	3.78	6.83	7.56
$D_{ax}{}^a \cdot 10^5$ [m^2·s^{-1}]	3.02	3.33	3.42	3.77	3.55	3.92	7.05	7.81
$D_p \cdot 10^5$ [m^2·s^{-1}]	2.99	3.33	3.49	3.88	3.65	4.06	8.11	9.02
k_f [m·s^{-1}]	0.0841	0.0933	0.0972	0.1077	0.1015	0.1125	0.2179	0.2415
$K_H(\mu_1)$ [mol·kg^{-1}·bar^{-1}]	67.4	45.6	1.19	0.650	9.30	4.00	0.0179	0.0142
K_H(fitting) [mol·kg^{-1}·bar^{-1}]	53.5	19.9	1.77	0.72	4.86	3.16	0.0317	0.0237
$D_c/r_c^2(D_{ax}) \cdot 10^2$ [s^{-1}][b]	0.0544	0.0753	1.85	2.59	0.491	0.848	12.0	14.3
$D_c/r_c^2(D_{ax}{}^a) \cdot 10^2$ [s^{-1}][b]	0.0577	0.0799	1.93	2.68	0.538	0.910	12.4	14.9
At 303 K: $Q = 6.38 \cdot 10^{-7}$ m^3·s^{-1}; $C_0 = 0.201$ mol·m^{-3} ($C_0 = 40.22$ mol·m^{-3} for H_2); $u_0 = 5.30 \cdot 10^{-2}$ m·s^{-1} ($u_0 = 5.47 \cdot 10^{-2}$ m·s^{-1} for H_2); $u_i = 2.12 \cdot 10^{-2}$ m·s^{-1} ($u_i = 2.16 \cdot 10^{-2}$ m·s^{-1} for H_2)								
At 323 K: $Q = 6.80 \cdot 10^{-7}$ m^3·s^{-1}; $C_0 = 0.189$ mol·m^{-3} ($C_0 = 37.73$ mol·m^{-3} for H_2); $u_0 = 5.65 \cdot 10^{-2}$ m·s^{-1} ($u_0 = 5.83 \cdot 10^{-2}$ m·s^{-1} for H_2); $u_i = 2.26 \cdot 10^{-2}$ m·s^{-1} ($u_i = 2.30 \cdot 10^{-2}$ m·s^{-1} for H_2)								

[a] The adsorbate partial pressure is 1 bar for H_2; for the other gases, it is 0.005 bar. [b] Estimated using a tortuosity factor, $\tau_p = 2$.

Literature Cited

(1) Bec, R. L. Method for purifying hydrogen-based gas mixtures using calcium X-zeolite. 6,849,106, February 1, 2005.

(2) Grande, C. A.; Lopes, F. V. S.; Ribeiro, A. M.; Loureiro, J. M.; Rodrigues, A. E. Adsorption of Off-Gases from Steam Methane Reforming (H2, CO2, CH4, CO and N2) on Activated Carbon. *Sep. Sci. Technol.* **2008**, *43* (6), 1338–1364.

(3) HY2SEPS Hybrid Hydrogen Carbon Dioxide Separation Processes. http://hy2seps.iceht.forth.gr/, 2005.

(4) Sircar, S.; Golden, T. C. Purification of Hydrogen by Pressure Swing Adsorption. *Sep. Sci. Technol.* **2000**, *35* (5), 667–687.

(5) Sircar, S.; Waldron, W. E.; Rao, M. B.; Anand, M. Hydrogen production by hybrid SMR-PSA-SSF membrane system. *Sep. Purif. Technol.* **1999**, *17*, 11–20.

(6) Yang, R. T. *Adsorbents: Fundamentals and Applications*; John Wiley & Sons, Inc.: Hoboken, NJ, 2003.

(7) Ahn, H.; Lee, C.-H.; Seo, B.; Yang, J.; Baek, K. Backfill Cycle of a Layered Bed H2 PSA Process. *Adsorption* **1999**, *5*, 419–433.

(8) Esteves, I. A. A. C.; Mota, J. P. B. Simulation of a new hybrid membrane/pressure swing adsorption process for gas separation. *Desalination* **2002**, *148*, 275–280.

(9) Ruthven, D. M.; Farooq, S.; Knabel, K. S. *Pressure Swing Adsorption*; VCH Publishers: New York, 1994.

(10) Wagner, J. L.; Lackawanna, N. Y. Selective adsorption process. 3,430,418, March 4, 1969.

(11) Yang, J.; Lee, C.-H. Adsorption Dynamics of a Layered Bed PSA for H2 Recovery from Coke Oven Gas. *AIChE J.* **1998**, *44* (6), 1325–1334.

(12) Zhou, L.; Lü, C.-Z.; Bian, S.-J.; Zhou, Y.-P. Pure Hydrogen from the Dry Gas of Refineries via a Novel Pressure Swing Adsorption Process. *Ind. Eng. Chem. Res.* **2002**, *41* (21), 5290–5297.

(13) Yang, J.; Han, S.; Cho, C.; Lee, C.-H.; Lee, H. Bulk separation of hydrogen mixtures by a one-column PSA process. *Sep. Technol.* **1995**, *5*, 239–349.

(14) Malek, A.; Farooq, S. Hydrogen Purification from Refinery Fuel Gas by Pressure Swing Adsorption. *AIChE J.* **1998**, *44* (9), 1985–1992.

(15) Park, J.-H.; Kim, J.-N.; Cho, S.-H. Performance analysis of a four-bed H2 PSA process using layered beds. *AIChE J.* **2000**, *46*, 790–802.

(16) Lee, J.-J.; Kim, M.-K.; Lee, D.-G.; Ahn, H.; Kim, M.-J.; Lee, C.-H. Heat-Exchange Pressure Swing Adsorption Process for Hydrogen Separation. *AIChE J.* **2008**, *54* (8), 2054–2064.

(17) Castaldi, P.; Santona, L.; Cozza, C.; Giuliano, V.; Abbruzzese, C.; Nastro, V.; Melis, P. Thermal and spectroscopic studies of zeolites exchanged with metal cations. *J. Mol. Struct.* **2005**, *734*, 99–105.

(18) Breck, D. W., *Zeolite Molecular Sieves*; R. E. Krieger Publishing: Malabar, FL, 1998.

(19) Hutson, N. D.; Rege, S. U.; Yang, R. T. Mixed cation zeolites: LixAgy-X as a superior adsorbent for air separation. *AIChE J.* **1999**, *45* (4), 724–734.

(20) Ursini, O.; Lilla, E.; Montanari, R. The investigation on cationic exchange capacity of zeolites: The use as selective ion trappers in the electrokinetic soil technique. *J. Hazard. Mater.* **2006**, *B 137* (2), 1079–1088.

(21) Jia, C.; Beaunier, P.; Massiani, P. Comparison of conventional and solid-state ion exchange procedures for the incorporation of lanthanum in H-beta zeolite. *Microporous Mesoporous Mater.* **1998**, *24* (1−3), 69–82.

(22) Golden, T. C.; Kumar, R.; Kratz, W. C. Hydrogen purification. 4,957,514, September 18, 1990.

(23) Coe, C. G.; Kirner, J. F.; Pierantozzi, R.; White, T. R. Nitrogen adsorption with Ca and or Sr exchanged lithium X-zeolites. 5,152,813, October 6, 1992.

(24) Plee, D. Purification of hydrogen flowstreams by selectively adsorbing impurities therefrom. 6,464,756, October 15, 2002.

(25) Reiss, G. Molecular sieve zeolite for producing hydrogen by pressure variation adsorption technique. 4,477,267, October 16, 1984.

(26) Bird, R. B.; Stewart, W. E.; Lightfoot, E. N. *Transport Phenomena*, 2nd ed.; Wiley Imternational: Singapore, 2002.

(27) Ruthven, D. M. *Principal of adsorption and adsorption processes*; John Wiley & Sons: New York, 1984.

(28) Wilke, C. R. Diffusional properties of multicomponent gases. *Chem. Eng. Prog.* **1950**, *46*, 95–104.

(29) Cavenati, S.; Grande, C. A.; Rodrigues, A. E. Separation of CH4/CO2/N2 Mixtures by Layered Pressure Swing Adsorption for Upgrade of Natural Gas. *Chem. Eng. Sci.* **2006**, *61*, 3893–3906.

(30) Dreisbach, F.; Staudt, R.; Keller, J. U. High Pressure Adsorption Data of Methane, Nitrogen, Carbon Dioxide and Their Binary and Ternary Mixtures on Activated Carbon. *Adsorption* **1999**, *5*, 215–227.

(31) Barrer, R. M. Sorption in porous crystals: equilibria and their interpretation. *J. Chem. Technol. Biotechnol.* **1981**, *31* (2), 71–85.

(32) Kiselev, A. V. Vapor adsorption on zeolites considered as crystalline species adsorbents. *Mol. Sieve Zeolites-II* **1971**, *102*, 37.

(33) Taqvi, S. M.; LeVan, M. D. Virial Description of Two-Component Adsorption on Homogeneous and Heterogeneous Surfaces. *Ind. Eng. Chem. Res.* **1997**, *36* (6), 2197–2206.

(34) Do, D. D. *Adsorption Analysis: Equilibria and Kinetics*; Imperial College Press: London, 1998; Vol. 2.
(35) Malek, A.; Farooq, S. Comparison of isotherm models for hydrocarbon adsorption on activated carbon. *AIChE J.* **1996**, *42* (11), 3191–3201.
(36) Bar, N.-K.; McDaniel, P. L.; Coe, C. G.; Seiffert, G.; Karger, J. Measurement of intracrystalline diffusion of nitrogen in zeolites NaX and NaCaA using pulsed field gradient n.m.r. *Zeolites* **1997**, *18* (1), 71–74.
(37) Caro, J.; Bülow, M.; Kärger, J. Comment on hydrocarbon diffusivity in zeolites. *Chem. Eng. Sci.* **1985**, *40* (11), 2169–2170.
(38) Kärger, J.; Ruthven, D. M. *Diffusion in Zeolites and Other Microporous Solids*, 1st ed.; John Wiley & Sons: New York, 1992.
(39) Sircar, S.; Waldron, W. E. Oxygen production by adsorption. 1 214 964 A2, June 19, 2002.
(40) Cavenati, S.; Grande, C. A.; Rodrigues, A. E. Adsorption Equilibrium of Methane, Carbon Dioxide, and Nitrogen on Zeolite 13X at High Pressures. *J. Chem. Eng. Data* **2004**, *49*, 1095–1101.
(41) Dantas, T. L. P.; Rezende, R. V. P.; Rodrigues, A. E.; Moreira, R. F. P. M., Adsorção de CO2 e N2 sobre carvão ativado e zeólita 13X: Isotermas de Equilíbrio através de medidas gravimétricas. In *7° Encontro Brasileiro sobre Adsorção - EBA*; Campina Grande - PB: Brasil, 2008.
(42) Ko, D.; Siriwardane, R.; Biegler, L. T. Optimization of a Pressure-Swing Adsorption Process Using Zeolite 13X for CO2 Sequestration. *Ind. Eng. Chem. Res.* **2003**, *42* (2), 339–348.
(43) Siriwardane, R. V.; Shen, M.-S.; Fisher, E. P. Adsorption of CO2 on zeolites at moderate temperature. *Energy Fuels* **2005**, *19*, 1153–1159.

Received for review March 26, 2009. Accepted September 4, 2009. The authors would like to thank financial support from European Project HY2SEPS (Hybrid Hydrogen - Carbon Dioxide Separation Systems), contract No. 019887.

JE900303Y